

A CENSUS OF THE TW HYA ASSOCIATION WITH GAIA¹

K. L. LUHMAN^{2,3}

Draft version May 8, 2023

ABSTRACT

I have used high-precision photometry and astrometry from the third data release of Gaia to perform a survey for members of the TW Hya association (TWA). I have identified candidate members that appear to share similar kinematics and ages with bona fide members compiled by Gagné et al. (2017) and I have assessed their membership using radial velocities and spectroscopic diagnostics of age from various sources. My new catalog of adopted members contains 67 Gaia sources in 55 systems. The histogram of spectral types for TWA peaks near M5 ($\sim 0.15 M_{\odot}$), resembling the distributions measured for other nearby young associations. The *UVW* velocities of its members indicate that the association is expanding. The rate of expansion corresponds to an age of $9.6_{-0.8}^{+0.9}$ Myr. In a Gaia color-magnitude diagram, the members of TWA exhibit well-defined sequences of single stars and unresolved binary stars. The combined sequence of low-mass stars in TWA is indicative of an age of $11.4_{-1.2}^{+1.3}$ Myr when compared to the sequence for Upper Centaurus-Lupus/Lower Centaurus-Crux, for which an age of 20 Myr is assumed. Based on these expansion and isochronal ages, I have adopted an age of 10 ± 2 Myr for TWA. Finally, I have used mid-infrared photometry from the Wide-field Infrared Survey Explorer to check for excess emission from circumstellar disks among the TWA members. Fourteen members have detected disks, all of which have been reported in previous studies. The fraction of members at $\leq M6$ ($\gtrsim 0.1 M_{\odot}$) that have full, transitional, or evolved disks is $10/52 = 0.19_{-0.06}^{+0.08}$. That value is similar to the fraction previously measured for the Upper Sco association, which is roughly coeval with TWA.

1. INTRODUCTION

Because of its proximity and youth (~ 40 – 100 pc, 10 Myr), the TW Hya association (TWA) is one of the most important stellar populations in the solar neighborhood. TW Hya was identified as a possible young star based on H α emission (Henize 1976) and it was confirmed as such through the detection of Li absorption at 6708 Å and additional emission lines (Herbig 1978; Rucinski & Krautter 1983). Candidates for young stars associated with TW Hya have been selected via their positions near sources detected by the Infrared Astronomical Satellite (de la Reza et al. 1989; Gregorio-Hetem et al. 1992; Zuckerman & Becklin 1993), X-ray emission (Kastner et al. 1997; Jensen et al. 1998; Sterzik et al. 1999; Webb et al. 1999; Zuckerman et al. 2001; Song et al. 2003; Looper et al. 2010a), UV emission (Rodríguez et al. 2011; Shkolnik et al. 2011; Binks et al. 2020), and optical and infrared (IR) colors (Gizis 2002; Scholz et al. 2005; Looper et al. 2007, 2010b; Schneider et al. 2012b, 2016; Gagné et al. 2014, 2017; Kellogg et al. 2015), often in conjunction with proper motions measured from wide-field imaging surveys. For some of those candidates, membership in TWA has been further constrained using measurements of radial velocities (e.g., Reid 2003; Torres et al. 2003;

Elliott et al. 2014; Malo et al. 2014; Kellogg et al. 2016; Kidder et al. 2019), parallaxes (Biller & Close 2007; Gizis et al. 2007; Ducourant et al. 2008; Teixeira et al. 2008; Ducourant et al. 2014; Weinberger et al. 2013; Donaldson et al. 2016; Best et al. 2020), and the moving cluster distance (Mamajek 2005). In one of the more recent membership studies of TWA, Gagné et al. (2017) classified 24 and 11 systems as bona fide members and high-likelihood candidates, respectively.

The identification of members of nearby associations has been greatly facilitated by the Gaia mission (Perryman et al. 2001; de Bruijne 2012; Gaia Collaboration et al. 2016), which is measuring high-precision photometry, proper motions, and parallaxes for more than a billion stars down to $G \sim 20$, corresponding to masses of ~ 0.01 – $0.015 M_{\odot}$ in TWA (Baraffe et al. 2015; Chabrier et al. 2023). Gagné & Faherty (2018) used the second data release of Gaia (DR2) to identify candidate members of 27 nearby associations, including nine candidates for TWA, most of which have lacked the spectroscopy needed for confirmation of membership.

In this paper, I use the third data release of Gaia (DR3, Gaia Collaboration et al. 2021, 2022) to identify candidate members of TWA and I assess their membership with spectra and radial velocity measurements from various sources. I then use my catalog of adopted members to study the association in terms of its initial mass function (IMF), kinematic and isochronal ages, and circumstellar disks.

2. SEARCH FOR NEW MEMBERS OF TWA

2.1. Identification of Candidate Members

¹ Based on observations made with the Gaia mission, the Two Micron All Sky Survey, the Wide-field Infrared Survey Explorer, Gemini Observatory, and European Southern Observatory telescopes at La Silla and Paranal Observatories.

² Department of Astronomy and Astrophysics, The Pennsylvania State University, University Park, PA 16802, USA; kll207@psu.edu

³ Center for Exoplanets and Habitable Worlds, The Pennsylvania State University, University Park, PA 16802, USA

For my survey of TWA, I have used the following data from Gaia DR3: photometry in bands at 3300–10500 Å (G), 3300–6800 Å (G_{BP}), and 6300–10500 Å (G_{RP}); proper motions and parallaxes ($G \lesssim 20$); and radial velocities ($G \lesssim 15$). For parallactic distances, I adopt the geometric values estimated by Bailer-Jones et al. (2021) from the DR3 parallaxes. In addition, I have made use of photometry in three near-IR bands (JHK_s) from the Point Source Catalog of the Two Micron All Sky Survey (2MASS, Skrutskie et al. 2003, 2006) and photometry in four mid-IR bands from the AllWISE Source Catalog of the Wide-field Infrared Survey Explorer (WISE, Wright et al. 2010, 2013; Cutri et al. 2013). The WISE bands are centered at 3.4, 4.6, 12, and 22 μm , which are denoted as W1, W2, W3, and W4, respectively. For members of TWA, 2MASS is slightly deeper than Gaia, and WISE is deeper than both 2MASS and Gaia.

As done in my previous surveys of young associations (e.g., Esplin & Luhman 2017; Luhman & Esplin 2020; Luhman 2022a), I have analyzed the Gaia astrometry in terms of a “proper motion offset” ($\Delta\mu_{\alpha,\delta}$), which is defined as the difference between the observed proper motion of a star and the motion expected at the celestial coordinates and parallactic distance of the star for a specified space velocity. The use of this metric minimizes projection effects, which is important for associations like TWA that cover a large area of sky. For my survey of TWA, the proper motion offsets are calculated relative to the motions expected for a velocity of $U, V, W = -12, -18, -6 \text{ km s}^{-1}$, which approximates the median velocity of TWA members (Gagné et al. 2017, Section 2.3).

To perform a census of TWA, I began by considering the most probable members from previous work. In a detailed study of TWA, Gagné et al. (2017) compiled a sample of 30 objects in 24 systems that they classified as bona fide members of TWA. While presenting an update to their algorithm for identifying members of young associations, Gagné et al. (2018) also included a list of bona fide TWA members, which was the same as in Gagné et al. (2017) except for the exclusion of TWA 9 by the newer study. I find that the data for TWA 9 are consistent with those of the other bona fide members, so I have used the sample from Gagné et al. (2017) to guide my survey.

In the top row of Figure 1, I have plotted the bona fide TWA members from Gagné et al. (2017) in diagrams of $\Delta\mu_{\alpha}$ versus right ascension and $\Delta\mu_{\delta}$ versus declination. A correlation is present in each diagram, which is suggestive of expansion. The expansion of TWA is better characterized through analysis of UVW velocities in Sections 2.3 and 3.2. The outliers among the bona fide members in Figure 1 are components of binary systems. Among those outliers, the components of a given binary tend to straddle the bulk of the bona fide members (i.e., the average proper motion offsets of a binary’s components are consistent with the overall population). In the top row of Figure 2, I show the bona fide TWA members in color-magnitude diagrams (CMDs) consisting of $M_{G_{RP}}$ versus $G_{BP} - G_{RP}$ and $G - G_{RP}$. I have excluded photometry with errors greater than 0.1 mag. The errors for TWA 30A exceed that threshold in G_{BP} and G_{RP} , so it does not appear in either CMD. For

comparison, I have included in each CMD a fit to the single-star sequence of the Pleiades cluster ($\sim 120 \text{ Myr}$, Stauffer et al. 1998; Dahm 2015) from Luhman (2023). TW Hya (TWA 1) is slightly fainter than the sequence formed by other members in the $G_{BP} - G_{RP}$ CMD while TWA 30B is well below the sequence in both CMDs. The former is likely caused by UV excess emission related to accretion (Rucinski & Krautter 1983; Muzerolle et al. 2000) and the latter may be evidence of an edge-on disk (Looper et al. 2010b).

To identify candidate members of TWA, I selected sources from Gaia DR3 that (1) are located within a spatial volume extending well beyond the bona fide members but that do not overlap with candidate members of Upper Centaurus-Lupus/Lower Centaurus-Crux (UCL/LCC) from Luhman (2022a) (see Section 2.3), (2) have proper motion offsets that are similar to those of the bona fide members or that are consistent with their pattern of expansion when extended in equatorial coordinates, and (3) appear near or above the lower envelope of the sequence of bona fide members in at least one CMD and do not appear below the sequence in either CMD. Since stars with disks can appear underluminous in CMDs, as mentioned earlier for TWA 1 and TWA 30B, I also considered Gaia sources that satisfied the first two criteria, appeared below the sequence in a CMD, and exhibited mid-IR excess emission in data from WISE. For the resulting candidates, I searched data archives and previous studies for spectroscopic measurements of age diagnostics (e.g., Li) and radial velocities. When spectroscopy was unavailable, I pursued new observations to measure spectral types and age diagnostics (Section 2.2). I rejected candidates if spectroscopy indicated ages older than those of the bona fide members or if radial velocity measurements and Gaia astrometry produced UVW velocities that are inconsistent with membership (Section 2.3). In the end, I arrived at a catalog of 67 adopted TWA members that have entries in Gaia DR3, which consist of 35 Gaia sources in 24 systems that correspond to the bona fide members from Gagné et al. (2017) and 32 additional Gaia sources in 31 systems. One of these sources, TWA 32B, has an entry in Gaia DR3 but lacks a parallax measurement. The companions TWA 2B and TWA 27B are absent from my catalog since they lack Gaia detections. Gaia usually detects both components of a pair like TWA 2A and 2B, which has a separation of $0''.56$ and $\Delta K = 0.8$ (Webb et al. 1999). TWA 27B has a wider separation of $0''.78$ from its primary (Chauvin et al. 2004), which is a brown dwarf (Gizis 2002), but a detection by Gaia is not expected given its very low luminosity.

To show the proper motion offsets and CMDs for my full catalog of adopted members, I have included them in the bottom rows of Figures 1 and 2. In the $G_{BP} - G_{RP}$ CMD, the TWA members exhibit a narrow, well-defined lower sequence that likely consists of single stars. An elevated sequence is evident as well, which likely corresponds to unresolved binaries. To my knowledge, (1) these CMDs are the first to resolve the single- and double-star sequences in TWA and (2) TWA is one of the youngest populations in which that has been done. The sequences of young stellar populations in CMDs and other versions of Hertzsprung-Russell (H-R) diagrams are broadest in star-forming regions and become more narrow at older ages, likely because of decreasing vari-

ability from spots and accretion, the removal of most extinction as the natal cloud disperses, and the fact that a given age spread corresponds to a smaller range of luminosities at older ages. As a result, detecting separate sequences for single and binary stars is more easily done with older populations. Doing so is also facilitated by accurate photometry, precise relative distances for the members of a population, and low contamination from nonmembers. Relative to most other clusters and associations, TWA has more accurate photometry and distances because of its proximity and less (negligible) variable extinction because of its location within the Local Bubble. In comparison, the single- and double-star sequences for Upper Sco and UCL/LCC (10 and 20 Myr) are less distinct than those in TWA (Luhman 2022a), likely because of variable extinction. In addition, since they are much richer and have more complex structure, Upper Sco and UCL/LCC may not have the same degree of coevality as a small group like TWA.

Unlike the $G_{\text{BP}} - G_{\text{RP}}$ CMD, the CMD for $G - G_{\text{RP}}$ contains a large group of stars that are significantly redder than the TWA sequences for single stars or binaries. Nearly all of those stars appear in the elevated sequence of unresolved binaries in the $G_{\text{BP}} - G_{\text{RP}}$ CMD, which is why the binary sequence is less populated in $G - G_{\text{RP}}$. G -band fluxes can be underestimated for extended sources (Riello et al. 2021), which would explain the anomalous colors of those TWA members if they are marginally resolved binaries.

When they were discovered, the young L dwarfs WISEA J114724.10–204021.3 and 2MASS J11193254–1137466 were classified as likely members of TWA (Kellogg et al. 2015, 2016; Schneider et al. 2016), but more recent astrometry appears to be inconsistent with membership (Best et al. 2020). Both objects are too faint for detections by Gaia, so I have calculated their proper motion offsets using the most accurate proper motions that are available (Best et al. 2018), a parallactic distance for WISEA J114724.10–204021.3 (Best et al. 2020), and a photometric distance for 2MASS J11193254–1137466 (Kellogg et al. 2015; Best et al. 2017). The resulting offsets are $(\Delta\mu_{\alpha}, \Delta\mu_{\delta}) = (-9 \pm 12, -32 \pm 5)$ and $(-7^{+31}_{-52}, -39^{+14}_{-24})$ mas yr⁻¹ for WISEA J114724.10–204021.3 and 2MASS J11193254–1137466, respectively, which differ significantly from the measurements for bona fide TWA members (Figure 1), supporting the results of Best et al. (2020).

2.2. Spectroscopy of Candidates

For candidate members of TWA that lack spectral classifications from previous studies, I have searched for spectra in the data archives of various observatories. I found optical spectra of five candidates that were obtained with the Fibre-fed Optical Echelle Spectrograph (FEROS; Kaufer et al. 1999) on the MPG/ESO 2.2 m telescope through program 090.C-0200(A), the Gemini Multi-Object Spectrograph (GMOS; Hook et al. 2004) at the Gemini South telescope through program GS-2014A-Q-44, and the Ultraviolet and Visual Echelle Spectrograph (UVES; Dekker et al. 2000) on the Unit Telescope 2 of the Very Large Telescope through program 092.C-0203(A). David Rodriguez was the principal investiga-

tor for each of the three programs. For eight remaining candidates that lacked archival spectra, I obtained data with GMOS at the Gemini South telescope. All of the spectra in question cover a wide range of wavelengths, spanning from 6000–9000 Å at a minimum. The data from GMOS, UVES, and FEROS exhibit $R \sim 4400$, 20,000, and 48,000, respectively. An example of one of the GMOS spectra is shown in Figure 3. All of the reduced spectra from GMOS are available in an electronic file associated with that figure. Pipeline-reduced spectra for UVES and FEROS can be retrieved from the data archive of the European Southern Observatory.

The 13 candidates with spectra are listed in Table 1. I have assessed the ages of the targets using Li absorption at 6707 Å and the Na doublet near 8190 Å, which is sensitive to surface gravity. In all of the spectra, the Na doublet is weak enough to be consistent with a pre-main-sequence star ($\lesssim 50$ Myr). Ten of the stars have sufficiently strong Li absorption (Table 1) to be near the age of TWA or younger (e.g., Mentuch et al. 2008). Two stars, which are components of a 2'' pair, have upper limits on the strength of Li that are inconsistent with membership (< 0.1 Å), so they are treated as nonmembers. The final candidate, which is the coolest one (M6), lacks a useful constraint on Li. For that star, I take the Na doublet as sufficient evidence of youth for inclusion in the catalog of members. I have measured spectral types for the candidates through comparison to field dwarf standards for $< M5$ (Henry et al. 1994; Kirkpatrick et al. 1991, 1997) and averages of dwarf and giant standards for $\geq M5$ (Luhman et al. 1997; Luhman 1999). The resulting classifications range from M3.5–M6 and are included in Table 1.

2.3. UVW Velocities

The membership of the TWA candidates selected from Gaia DR3 in Section 2.1 can be further constrained via UVW velocities if they have measurements of radial velocities. I have compiled previous measurements of radial velocities for the bona fide members of TWA from Gagné et al. (2017) and the additional candidate members. For most stars that have multiple radial velocity measurements, I have adopted the velocity with the smallest error. In the case of Gaia DR3 3567379121431731328, the measurements span a range of ~ 20 km s⁻¹, which is much larger than the individual errors (1–3 km s⁻¹, Gagné et al. 2017; Riedel et al. 2017, Gaia DR2 and DR3) and is suggestive of a spectroscopic binary. For the purpose of calculating the UVW velocity, I have adopted the radial velocity from Gaia DR3, which is near the middle of the velocity range. For TWA 4A, I have used a measurement of the radial velocity for the TWA 4A+B system (Zúñiga-Fernández et al. 2021b). TWA 23 is a spectroscopic binary that exhibits significant variation in its radial velocity measurements (Shkolnik et al. 2011; Bailey et al. 2012). Zúñiga-Fernández et al. (2021a) calculated the median and standard deviation of its available velocities, which I have adopted. Gaia DR3 provides separate velocities for the components of the 0'58 pair TWA 16 while a much more precise measurement is available for the composite of the system from Zúñiga-Fernández et al. (2021a). The latter measure-

ment has been adopted for the primary. Similarly, I have assigned the unresolved radial velocity measurement for the 0^h66 pair TWA 32 to its primary. The secondary in that system is the only bona fide member that lacks a radial velocity in my catalog.

I have used the radial velocities in conjunction with proper motions from Gaia DR3 and parallactic distances based on DR3 parallaxes (Bailer-Jones et al. 2021) to calculate UVW velocities (Johnson & Soderblom 1987). The velocity errors were estimated in the manner described by Luhman & Esplin (2020) using the python package `pyia` (Price-Whelan 2021).

To illustrate their spatial distribution, I have plotted the bona fide TWA members from Gagné et al. (2017) in diagrams of XYZ Galactic Cartesian positions in the top row of Figure 4. In the diagram of Y versus X , I have included a boundary that approximates the edge of the UCL/LCC members identified by Luhman (2022a). TWA and UCL/LCC overlap in Z , so similar boundaries are not shown in the other two diagrams of spatial positions. As mentioned in Section 2.1, I have excluded the volume encompassing UCL/LCC from my survey for TWA members.

In the bottom row of Figure 4, the measurements of U , V , and W for the bona fide TWA members are plotted versus X , Y , and Z , respectively. Most of the stars are well-clustered in those diagrams. The outliers are components of binary systems and their binarity likely accounts for the discrepant velocities. The velocity components of the bona fide members are correlated with their corresponding spatial dimensions, which indicates the presence of expansion, as found with the proper motion offsets in Figure 1 (Section 2.1). In my survey for new members, I have excluded stars that have UVW velocities that do not follow the pattern of expansion of the bona fide members, as discussed in Section 2.1.

In Figure 5, I present diagrams of XYZ and UVW for the bona fide members and the additional stars that I have adopted as members. The latter span a larger spatial volume than the former. The range of distances among the adopted members is 34–105 pc. All else being equal, spatial outliers are more likely than centrally concentrated candidates to be contaminants, so I have flagged the outliers in the catalog presented in Table 2. Ten of the adopted members are absent from the diagrams of UVW since they lack radial velocity data. One of them, TWA 32B, is a secondary in a system that has a measured radial velocity. Measurements of the radial velocities for the remaining nine stars would help to better constrain their membership. In addition, the available radial velocities for two of the coolest members, 2MASS J12474428–3816464 and TWA 40, have large uncertainties (6 and 7 km s⁻¹), so their membership constraints would benefit from more accurate measurements. For the 57 adopted members that have measured UVW velocities, the median velocity is $U, V, W = -12.2, -18.4, -6.1$ km s⁻¹.

The 67 Gaia sources that are adopted as TWA members in this work are presented in Table 2, which includes source names from Gaia DR3 and previous studies; equatorial coordinates, proper motion, parallax, renormalized unit weight error (RUWE, Lindegren 2018), and photometry from Gaia DR3; measurements of spectral types and the type adopted in this work; distance estimate based

on the Gaia DR3 parallax (Bailer-Jones et al. 2021); the adopted radial velocity measurement; the UVW velocities calculated in this section; the designations and angular separations of the closest sources within 3^h from 2MASS and WISE; flags indicating whether the Gaia source is the closest match in DR3 for the 2MASS and WISE sources; photometry from 2MASS and WISE (only for the Gaia source that is closest to the 2MASS/WISE source); flags indicating whether excesses are detected in three WISE bands and a disk classification if excess emission is detected (Section 3.4); a flag for the bona fide members from Gagné et al. (2017); and a flag for spatial outliers (Figure 5). TWA 16, TWA 32, and TWA 39 are binaries with separations of $\lesssim 1''$ in which the components have similar apparent magnitudes from Gaia. For each system, the spectral classification is based on seeing-limited data and likely applies to a composite of both components. I have assigned those spectral types to the primaries in Table 2.

2.4. Comparison to Previous Studies

I discuss two stars that are among my adopted TWA members but that have been rejected in some previous studies: Gaia DR3 3567379121431731328 and TWA 31. The former was rejected by Gagné et al. (2017), likely because of their measurement of its radial velocity (-0.1 ± 0.8 km s⁻¹). When I adopt the value of 12.29 ± 4.15 km s⁻¹ from Gaia DR3, which is closer to the middle of the available measurements, the resulting UVW velocity is roughly consistent with membership (Figure 5). The star appears above the single-star sequence for TWA in the CMDs in Figure 2, which is consistent with the fact that it may be an unresolved binary based on its large spread in measured velocities and its spectrum (Gagné et al. 2017). I have included it in my catalog of adopted members, but a measurement of its system velocity would be useful for better assessing membership. The second star, TWA 31, was identified as a possible member of TWA by Shkolnik et al. (2011) but was classified as a likely contaminant from LCC by Gagné et al. (2017). More recently, Venuti et al. (2019) found that the UVW velocity of the star based on Gaia DR2 data was consistent with membership in TWA. I arrive at the same conclusion with the data from Gaia DR3. With a position near $X, Y, Z = 27, -66, 40$ pc, TWA 31 is not a spatial outlier compared to other TWA members and it does not overlap with UCL/LCC (Figure 5). The strength of its Li absorption indicates an age of < 20 Myr (Shkolnik et al. 2011), which is consistent with TWA membership. The presence of a circumstellar disk with a high accretion rate serves as additional evidence of youth (Shkolnik et al. 2011; Schneider et al. 2012a; Venuti et al. 2019). It is much fainter than other TWA members near its spectral type in the Gaia CMDs (Figure 2), which suggests that it is seen primarily in scattered light at optical wavelengths (e.g., edge-on disk).

Gagné et al. (2017) presented three categories of possible members of TWA. My catalog includes all of their bona fide members (35 Gaia sources in 24 systems), nine of their 12 high-likelihood candidate members (TWA 3A and B are counted separately), and five of their 44 candidate members. In addition, it contains four stars rejected for membership in TWA by that study (e.g., the aforementioned TWA 31

and Gaia DR3 3567379121431731328) and five of the nine TWA candidates identified with Gaia DR2 by Gagné & Faherty (2018). One remaining star, Gaia DR3 5412403269717562240, was classified as a member of the β Pic moving group by Schneider et al. (2019). It is a modest outlier in Z relative to other TWA members ($Z = 5$ pc), but its UVW velocity is consistent with membership when accounting for the pattern of expansion. It is also an outlier in Y and Z relative to members of β Pic (Shkolnik et al. 2017).

3. PROPERTIES OF THE TWA STELLAR POPULATION

3.1. Initial Mass Function

Previous catalogs of proposed members of TWA have been used to estimate the association’s IMF (Looper 2011; Gagné et al. 2017). The same can be done with my new catalog of adopted members. As in my previous surveys of star-forming regions and young associations, I have used spectral type as an observational proxy for stellar mass when characterizing the IMF of TWA. In Figure 6, I have plotted a histogram of spectral types for the TWA members. The source catalog from Gaia DR3 has a high level of completeness at $G \lesssim 19$ –20 for most of the sky (Boubert & Everall 2020; Fabricius et al. 2021). At the far side of the association (~ 100 pc), $G = 19$ corresponds to a spectral type of $\sim M8$ among members of TWA, so the histogram in Figure 6 should be unbiased for types earlier than that value. Two likely members that lack Gaia detections are absent from my catalog and thus do not appear in Figure 6 (Section 2.1), consisting of TWA 2B (M2–M3.5, Webb et al. 1999; Herczeg & Hillenbrand 2014) and TWA 27B (mid-to-late L, Chauvin et al. 2004; Mohanty et al. 2007; Patience et al. 2010; Allers & Liu 2013). The histogram of spectral types for TWA exhibits a maximum near M5 ($\sim 0.15 M_{\odot}$), which resembles the distributions measured for other nearby young associations (e.g., Luhman 2022a).

3.2. Kinematic Ages

Two forms of kinematic ages can be explored for young unbound associations, consisting of the expansion age and the traceback age (e.g., Blaauw 1964; Brown et al. 1997; Mamajek & Bell 2014; Crundall et al. 2019; Zari et al. 2019; Miret-Roig et al. 2020; Luhman 2022c; Couture et al. 2023; Galli et al. 2023). Previous studies have attempted to derive both ages for TWA (Makarov et al. 2005; Mamajek 2005; de la Reza et al. 2006; Ducourant et al. 2014; Donaldson et al. 2016). Kinematic age estimates in TWA should benefit significantly from the expanded size and improved membership classifications in the new TWA census, the high precision of the Gaia astrometry, and the availability of radial velocity data for most of the members. For my analysis of the kinematic ages, I have omitted the two members that have the largest radial velocity uncertainties, 2MASS J12474428–3816464 and TWA 40, and multiple systems that have discrepant velocities relative to other TWA members, which consist of TWA 4A/B, TWA 5A/B, and Gaia DR3 3567379121431731328 (Figure 5).

As mentioned in Section 2.3 and illustrated in Figure 5, the space velocities for the TWA members exhibit correlations with spatial positions, which indicate the presence

of expansion. The rate of expansion can be directly converted to an age under the assumption that the stars have traveled on linear trajectories. However, members of an expanding association will eventually experience acceleration due to the Galactic potential (Blaauw 1952). For an association near an age of 10 Myr, the effect on the expansion rates in X and Y should be negligible, but the rate in Z could differ by up to 20–30% from the value for linear expansion (Brown et al. 1997). I have estimated the slopes of the correlations between UVW and XYZ in Figure 5, which are the expansion rates, using robust linear regression with bootstrap sampling, arriving at 0.103 ± 0.012 , 0.099 ± 0.021 , and 0.101 ± 0.018 km s $^{-1}$ pc $^{-1}$ in X , Y , and Z , respectively. In studies of young associations, the XYZ expansion rates often are inconsistent with a single well-defined value, but the rates for TWA have fairly small errors and agree surprisingly well, including the rate in Z . The weighted mean of the three slopes is 0.102 ± 0.009 km s $^{-1}$ pc $^{-1}$, which corresponds to an expansion age of $9.6^{+0.9}_{-0.8}$ Myr. As done for the 32 Ori association in Luhman (2022c), I have also attempted to estimate a traceback age for TWA by identifying the times in the past when the standard deviations of X , Y , and Z were each minimized. The implied ages do not correspond to a single value and instead range from ~ 3 –8 Myr. It is possible that choosing a different metric for the size of the association would produce a better defined traceback age (Miret-Roig et al. 2020; Couture et al. 2023; Galli et al. 2023).

3.3. Isochronal Age

The age of a young association can be estimated from a comparison of its sequence of low-mass stars in an H-R diagram to isochrones from theoretical evolutionary models (Baraffe et al. 2015; Choi et al. 2016; Dotter 2016; Feiden 2016). Previous studies have applied that method to members of TWA, typically producing ages of ~ 8 –10 Myr (Stauffer et al. 1995; Soderblom et al. 1998; Webb et al. 1999; Barrado y Navascués 2006; Weinberger et al. 2013; Bell et al. 2015; Herczeg & Hillenbrand 2015; Donaldson et al. 2016). As with the kinematic ages, it should be possible to improve the estimate of the isochronal age of TWA with the new census.

To derive an isochronal age for TWA, I have followed the procedure applied to associations near the Taurus star-forming region in Luhman (2023). I have selected TWA members that have precise parallaxes ($\sigma_{\pi} < 0.1$ mas) and photometry ($\sigma_{BP} < 0.1$, $\sigma_{RP} < 0.1$) and have colors indicative of low-mass stars ($G_{BP} - G_{RP} = 1.4$ –2.8). Disk-bearing stars are excluded to avoid contamination of the photometry by disk-related emission. Within that color range, all members satisfy the criteria for photometric errors and only four of the diskless stars are omitted because of parallax errors. All of the latter are companions that have poor astrometric fits according to their large values of RUWE. The resulting sample contains 17 sources. I have calculated their offsets in M_{GRP} from a fit to the median of the sequence for UCL/LCC (Luhman 2023). I have assumed that the stars have no extinction since they are located within the Local Bubble. A histogram of the M_{GRP} offsets is shown in Figure 7. I have calculated the median and the me-

dian absolute deviation (MAD) of the offsets, arriving at -0.36 and 0.07 , respectively. If the criteria for parallax error or disks are eliminated, the median offset is nearly unchanged, but the MAD increases because most of the added stars are elevated above the single-star sequence (i.e., likely unresolved binaries). This is a reflection of the fact that the value of MAD is dominated by the intrinsic width of the TWA sequence produced by single and binary stars rather than measurement errors.

I have converted the median offset for the sample of 17 stars to an age by assuming that UCL/LCC ($\Delta M=0$) has an age of 20 Myr (Luhman 2022a) and that $\Delta \log L / \Delta \log \text{age} = -0.6$, as done in Luhman (2023). The age of 20 Myr for UCL/LCC is tied to the lithium depletion boundary (LDB) age for the β Pic moving group (Binks & Jeffries 2016), as discussed in Luhman (2022a). The resulting isochronal age for TWA is $11.4_{-1.2}^{+1.3}$ Myr. Once again, that error is determined primarily by the gap between the single- and double-star sequences and the relative numbers of singles and binaries in the sample. In addition, the derived age may be subject to systematic errors arising from the adopted age for UCL/LCC and the conversion from $M_{G_{\text{RP}}}$ offsets to relative ages.

As an alternative to the above approach, an age for TWA can be estimated by directly fitting its single-star sequence of low-mass stars in $M_{G_{\text{RP}}}$ versus $G_{\text{BP}} - G_{\text{RP}}$ with model isochrones. For instance, the isochrones of Baraffe et al. (2015) imply an age of ~ 6 Myr while the models of Dotter (2016) and Choi et al. (2016) imply an age of ~ 4 Myr. Models that account for the inhibition of convection by magnetic fields tend to produce older ages that are in better agreement with ages derived from the LDB and the mass-radius relationship for young low-mass stars (Kraus et al. 2015; David et al. 2016, 2019; Feiden 2016; MacDonald & Mullan 2017; Binks et al. 2022). However, in the Gaia CMD, new versions of the magnetic isochrones from Feiden (2016) provided by G. Feiden (private communication) are much less parallel to the TWA single-star sequence than the non-magnetic isochrones, implying ages of ~ 25 and 11 Myr at $G_{\text{BP}} - G_{\text{RP}} = 1.6$ and 3, respectively. Given these complications with the fitting of both non-magnetic and magnetic isochrones, I prefer the procedure followed earlier in this section in which empirical isochrones are compared and some are dated with the LDB (Herczeg & Hillenbrand 2015).

From this study, the most reliable age estimates for TWA appear to be the expansion age of $9.6_{-0.8}^{+0.9}$ Myr and the isochronal age of ~ 11.4 Myr. Based on these values, I adopt an age of 10 ± 2 Myr for TWA.

3.4. Circumstellar Disks

I have used mid-IR photometry from WISE to search for evidence of disks among the adopted members of TWA. The 67 objects in my catalog have 61 matching sources from WISE. If a close pair of Gaia sources has the same WISE source as their closest match, the WISE designation appears in both of their entries in Table 2, but the disk measurements from this section are listed only for the candidate that is closest to the WISE source. The AllWISE Atlas images of the WISE sources have been visually inspected to check for detections that are false or unreliable, which are marked by a flag in Table 2.

As done in my previous surveys of young associations (e.g., Luhman 2022b), I have used W1–W2, W1–W3, and W1–W4 to detect excess emission from disks among the 61 WISE sources in TWA. Those colors are plotted versus spectral type in Figure 8. I have omitted W2 data at $W2 < 6$ since they are subject to significant systematic errors (Cutri et al. 2012). In each of the three colors, some sources are found in a blue sequence that corresponds to stellar photospheres while others have redder colors that indicate the presence of IR excess emission from circumstellar dust. In Figure 8, I have marked the threshold for each color that was used by Luhman (2022b) for identifying color excesses. Flags indicating the presence or absence of excesses in W2, W3, and W4 are included in Table 2.

For two of the TWA members that lack detections in W4, TWA 8B and TWA 26, measurements in a similar band at $24 \mu\text{m}$ (denoted as [24]) with the Multiband Imaging Photometer for Spitzer (MIPS; Rieke et al. 2004; Werner et al. 2004) have been reported in previous studies (Riaz et al. 2006b; Luhman et al. 2010; Schneider et al. 2012a). I have adopted the MIPS data as a proxy for W4 when calculating W1–W4 and determining the excess flag for W4. Because of the proximity to its primary ($8''$), HR 4796B appears to have unreliable photometry in W2, W3, and W4. As a result, it is the only WISE source in my catalog that is not assessed for excess emission in any of those bands.

The evolutionary stages of the detected disks have been classified from among the following options: full disk, transitional disk, evolved disk, evolved transitional disk, and debris disk (Kenyon & Bromley 2005; Rieke et al. 2005; Hernández et al. 2007; Luhman et al. 2010; Espaillat et al. 2012). The classes are estimated based on the sizes of the excesses in $K_s - W3$ and $K_s - W4$ (Luhman & Mamajek 2012; Esplin et al. 2014, 2018). The color excesses, $E(K_s - W3)$ and $E(K_s - W4)$, are calculated by subtracting the expected photospheric color for a given spectral type (Luhman 2022a). The resulting excesses are plotted in Figure 9 with the criteria for the disk classes (Esplin et al. 2018). The values of $E(K_s - W2)$ are included as well to illustrate sizes of the excesses in W2. Sources that lack excesses in any of the WISE bands are excluded from Figure 9 and are designated as class III (Lada & Wilking 1984; Lada 1987). The excesses for TWA 30B are large enough to place it beyond the limits of Figure 9. Gaia DR3 6152893526035165312 has excesses in W2 and W3 but is not detected in W4, so it is absent from those diagrams. The excesses in Figure 9 imply that HR 4796 has a transitional disk and that TW Hya and HD 98800B have full disks, but more detailed measurements of their spectral energy distributions indicate that HR 4796 has a debris disk and the latter two stars have transitional disks (Jura 1991; Augereau et al. 1999; Calvet et al. 2002; Uchida et al. 2004; Furlan et al. 2007), which are the classes adopted in Table 2.

Fourteen of the WISE sources exhibit IR excess emission, all of which have had disks detected in previous work (Rucinski & Krautter 1983; de la Reza et al. 1989; Jura 1991; Gregorio-Hetem et al. 1992; Zuckerman & Becklin 1993; Mohanty et al. 2003; Sterzik et al. 2004; Uchida et al. 2004; Low et al. 2005; Riaz et al. 2006b; Morrow et al. 2008; Rebull et al. 2008;

Riaz & Gizis 2008; Herczeg et al. 2009; Looper et al. 2010a,b; Shkolnik et al. 2011; Schneider et al. 2012a,b; Rodriguez et al. 2015; Boucher et al. 2016; Binks & Jeffries 2017). They consist of four full, seven evolved, two transitional, and one debris disk. Previous studies have reported a modest excess in [24] for TWA 7 based on $K_s - [24]$ (Low et al. 2005; Rebull et al. 2008; Schneider et al. 2012a; Binks & Jeffries 2017), but I do not find an excess in either [24] or W4 relative to W1. The previous detections of an excess in [24] may have been caused by variability between the observations in K and the mid-IR bands. Similarly, Rebull et al. (2008) identified an excess in [24] for TWA 8B using $K_s - [24]$, whereas I find that W1-[24] is consistent with the expected photospheric value.

Among WISE sources in TWA that have been assessed for IR excesses and that have spectral types of $\leq M6$, the fraction that have full, transitional, or evolved disks is $10/52=0.19_{-0.06}^{+0.08}$. That value is consistent with the disk fraction for the same range of types in Upper Sco (0.19 ± 0.01 , Luhman 2022b), which is roughly coeval with TWA (Section 3.3, Luhman & Esplin 2020).

4. CONCLUSIONS

I have performed a survey for members of the TW Hya association using high-precision photometry and astrometry from Gaia DR3 and ground-based spectroscopy. I have used the new catalog of adopted members to characterize the IMF and the age of the association and to identify and classify its circumstellar disks. The results are summarized as follows:

1. Gagné et al. (2017) compiled a sample of bona fide members of TWA, consisting of 24 systems that are resolved into 35 sources in Gaia DR3. I have used the kinematics and photometry of those members to guide a search for additional members with Gaia DR3. For the resulting candidates, I have checked whether membership is supported by UVW velocities (when radial velocities are available) and spectroscopic diagnostics of age. All of the candidates have the latter from previous studies or new spectra analyzed in this work. In the end, my catalog of adopted members contains 67 Gaia sources in 55 systems. In addition to the bona fide members, the catalog includes nine high-likelihood candidates (eight systems) and five candidates from Gagné et al. (2017) and five candidates from Gagné & Faherty (2018). The remaining 13 adopted members have not been previously classified as candidates. Although all objects in the catalog have good evidence of membership from Gaia data and spectroscopy, measurements of radial velocities for the nine systems that lack such data would be useful for further assessing their membership.
2. The histogram of spectral types for the adopted members of TWA peaks near M5 ($\sim 0.15 M_{\odot}$), indicating that the characteristic mass of the IMF in TWA is similar to the values in other nearby associations and star-forming regions.
3. For the TWA members that have measured radial velocities, U , V , and W are positively correlated

with X , Y , and Z , respectively, indicating the presence of expansion. The slopes of the three correlations are consistent with each other and their weighted mean corresponds to an expansion age of $9.6_{-0.8}^{+0.9}$ Myr.

4. In a CMD constructed from Gaia data, the members of TWA exhibit well-defined sequences of single stars and unresolved binary stars. TWA is one of the youngest populations (if not the youngest) in which the two sequences have been resolved. The combined sequence of low-mass stars is 0.36 ± 0.07 mag brighter than the median sequence for UCL/LCC. If one adopts an age of 20 Myr for the latter and assumes that young low-mass stars fade at a rate given by $\Delta \log L / \Delta \log \text{age} = -0.6$, the offset for TWA from UCL/LCC corresponds to an age of $11.4_{-1.2}^{+1.3}$ Myr. Based on that value and the expansion age, I adopt an age of 10 ± 2 Myr for TWA.
5. I have used mid-IR photometry from WISE to identify TWA members that exhibit IR excesses from disks. The evolutionary stages of the detected disks have been classified using the sizes of the excesses. Fourteen members have IR excesses, all of which have had disks reported in previous studies. Among WISE sources in TWA that have been assessed for IR excesses and that have spectral types of $\leq M6$, the fraction that have full, transitional, or evolved disks is $10/52=0.19_{-0.06}^{+0.08}$. That value is consistent with the disk fraction for the same range of types in Upper Sco (0.19 ± 0.01 , Luhman 2022b), which is roughly coeval with TWA.

This work used data from the European Space Agency mission Gaia (<https://www.cosmos.esa.int/gaia>), processed by the Gaia Data Processing and Analysis Consortium (DPAC, <https://www.cosmos.esa.int/web/gaia/dpac/consortium>). Funding for the DPAC has been provided by national institutions, in particular the institutions participating in the Gaia Multilateral Agreement. The Gemini data were obtained through programs GS-2014A-Q-44 and GS-2023A-FT-20. Gemini Observatory is a program of NSF's NOIRLab, which is managed by the Association of Universities for Research in Astronomy (AURA) under a cooperative agreement with the National Science Foundation on behalf of the Gemini Observatory partnership: the National Science Foundation (United States), National Research Council (Canada), Agencia Nacional de Investigación y Desarrollo (Chile), Ministerio de Ciencia, Tecnología e Innovación (Argentina), Ministério da Ciência, Tecnologia, Inovações e Comunicações (Brazil), and Korea Astronomy and Space Science Institute (Republic of Korea). 2MASS is a joint project of the University of Massachusetts and IPAC at Caltech, funded by NASA and the NSF. WISE is a joint project of the University of California, Los Angeles, and the JPL/Caltech, funded by NASA. This work used data from the NASA/IPAC Infrared Science Archive, operated by JPL under contract with NASA, and the VizieR catalog access tool and the SIMBAD database, both operated at CDS, Strasbourg, France. The Center

for Exoplanets and Habitable Worlds is supported by the Pennsylvania State University, the Eberly College of Science, and the Pennsylvania Space Grant Consortium.

REFERENCES

- Abt, H. A., & Morrell, N. I. 1995, *ApJS*, 99, 135
- Allers, K. N., & Liu, M. C. 2013, *ApJ*, 772, 79
- Augereau, J. C., Lagrange, A. M., Mouillet, D., Papaloizou, J. C. B., & Grorod, P. A. 1999, *A&A*, 348, 557
- Bailer-Jones, C. A. L., Rybizki, J., Fouesneau, M., Demleitner, M., & Andrae, R. 2021, *AJ*, 161, 147
- Bailey, J. I., III, White, R. J., Blake, C. H., et al. 2012, *ApJ*, 749, 16
- Baraffe, I., Horneier, D., Allard, F., & Chabrier, G. 2015, *A&A*, 577, 42
- Barrado y Navascués, D. 2006, *A&A*, 459, 511
- Bell, C. P. M., Mamajek, E. E., & Naylor, T. 2015, *MNRAS*, 454, 593
- Best, W. M. J., Liu, M. C., Dupuy, T. J., & Magnier, E. A. 2017, *ApJ*, 843, L4
- Best, W. M. J., Liu, M. C., Magnier, E. A., & Dupuy, T. J. 2020, *AJ*, 159, 257
- Best, W. M. J., Magnier, E. A., Liu, M. C., et al. 2018, *ApJS*, 234, 1
- Bidelman, W. P., Ratcliff, S. J., & Svolopoulos, S. 1988, *PASP*, 100, 828
- Biller, B. A., & Close, L. M. 2007, *ApJ*, 669, L41
- Binks, A. S., Chalifour, M., Kastner, J. H., et al. 2020, *MNRAS*, 491, 215
- Binks, A. S., & Jeffries, R. D. 2016, *MNRAS*, 455, 3345
- Binks, A. S., & Jeffries, R. D. 2017, *MNRAS*, 469, 579
- Binks, A. S., Jeffries, R. D., Sacco, G. G., et al. 2022, *MNRAS*, 513, 5727
- Blaauw, A. 1952, *Bulletin of the Astronomical Institutes of the Netherlands*, 11, 414
- Blaauw, A. 1964, *ARA&A*, 2, 213
- Bonnefoy, M., Chauvin, G., Lagrange, A.-M., et al. 2014, *A&A*, 562, A127
- Boubert, D., & Everall, A. 2020, *MNRAS*, 497, 4246
- Boucher, A., Lafrenière, D., Gagné, J., et al. 2016, *ApJ*, 832, 50
- Bowler, B. P., Hinkley, S., Ziegler, C., et al. 2019, *ApJ*, 877, 60
- Brown, A. G. A., Dekker, G., & de Zeeuw, P. T. 1997, *MNRAS*, 285, 479
- Buder, S., Asplund, M., Duong, L., et al. 2018, *MNRAS*, 478, 4513
- Calvet, N., D'Alessio, P., Hartmann, L., et al. 2002, *ApJ*, 568, 1008
- Cannon, A. J., & Pickering, E. C. 1993, *yCat*, 3135, 0
- Chabrier, G., Baraffe, I., Phillips, M., & Debras, F. 2023, *A&A*, 671, A119
- Chauvin, G., Lagrange, A.-M., Dumas, C., et al. 2004, *A&A*, 425, L29
- Choi, J., Dotter, A., Conroy, C., et al. 2016, *ApJ*, 823, 102
- Couture, D., Gagné, J., & Doyon, R. 2023, *ApJ*, 946, 6
- Crundall, T. D., Ireland, M. J., Krumholz, M. R., et al. 2019, *MNRAS*, 489, 3625
- Cutri, R. M., Wright, E. L., Conrow, T., et al. 2012, *Explanatory Supplement to the WISE All-Sky Data Release Products*
- Cutri, R. M., Wright, E. L., Conrow, T., et al. 2013, *yCat*, 2328, 0C
- Dahm, S. E. 2015, *ApJ*, 813, 108
- David, T. J., Hillenbrand, L. A., Cody, A. M., Carpenter, J. M., & Howard, A. W. 2016, *ApJ*, 816, 21
- David, T. J., Hillenbrand, L. A., Gillen, E., et al. 2019, *ApJ*, 872, 161
- de Bruijne, J. H. J. 2012, *Ap&SS*, 341, 31
- Dekker, H., D'Odorico, S., Kaufer, A., Delabre, B., & Kotzłowski, H. 2000, *SPIE*, 4008, 534
- de la Reza, R., Jilinski, E., & Ortega, V. G. 2006, *AJ*, 131, 2609
- de la Reza, R., Torres, C. A. O., Quast, G., Castilho, B. V., & Vieira, G. L. 1989, *ApJ*, 343, L61
- Donaldson, J. K., Weinberger, A. J., Gagné, J., et al. 2016, *ApJ*, 833, 95
- Dotter, A. 2016, *ApJS*, 222, 8
- Ducourant, C., Teixeira, R., Chauvin, G., et al. 2008, *A&A*, 477, L1
- Ducourant, C., Teixeira, R., Galli, P. A. B., et al. 2014, *A&A*, 563, A121
- Elliott, P., Bayo, A., Melo, C. H. F., et al. 2014, *A&A*, 568, A26
- Espallat, C., Ingleby, L., Hernandez, J., et al. 2012, *ApJ*, 747, 103
- Esplin, T. L., & Luhman, K. L. 2017, *AJ*, 154, 134
- Esplin, T. L., Luhman, K. L., & Mamajek, E. E. 2014, *ApJ*, 784, 126
- Esplin, T. L., Luhman, K. L., Miller, E. B., & Mamajek, E. E. 2018, *AJ*, 156, 75
- Fabricius, C., Luri, X., Arenou, F., et al. 2021, *A&A*, 649, A5
- Feiden, G. A. 2016, *A&A*, 593, A99
- Fouqué, P., Moutou, C., Malo, L., et al. 2018, *MNRAS*, 475, 1960
- Furlan, E., Sargent, B., Calvet, N., et al. 2007, *ApJ*, 664, 1176
- Gagné, J., & Faherty, J. K. 2018, *ApJ*, 862, 138
- Gagné, J., Faherty, J. K., Cruz, K. L., et al. 2014, *ApJ*, 785, L14
- Gagné, J., Faherty, J. K., Cruz, K. L., et al. 2015, *ApJS*, 219, 33
- Gagné, J., Faherty, J. K., Mamajek, E. E., et al. 2017, *ApJS*, 228, 18
- Gagné, J., Mamajek, E. E., Malo, L., et al. 2018, *ApJ*, 856, 23
- Gaia Collaboration, Brown, A. G. A., Vallenari, A., Prusti, T., et al. 2021, *A&A*, 649, A1
- Gaia Collaboration, Prusti, T., de Bruijne, J. H. J., et al. 2016, *A&A*, 595, A1
- Gaia Collaboration, Vallenari, A., Brown, A. G. A., et al. 2022, *arXiv:2208.00211*
- Galli, P. A. B., Miret-Roig, N., Bouy, H., Olivares, J., & Barrado, D. 2023, *MNRAS*, 520, 6245
- Gizis, J. E. 2002, *ApJ*, 575, 484
- Gizis, J. E., Jao, W.-C., Subasavage, J. P., & Henry, T. J. 2007, *ApJ*, 669, L45
- Gregorio-Hetem, J., Lépine, J. R. D., Quast, G. R., Torres, C. A. O., & de la Reza, R. 1992, *AJ*, 103, 549
- Hawley, S. L., Gizis, J. E., & Reid, I. N. 1996, *AJ*, 112, 2799
- Henize, K. G. 1976, *ApJS*, 30, 491
- Henry, T. J., Kirkpatrick, J. D., & Simons, D. A. 1994, *AJ*, 108, 1437
- Herbig, G. H. 1978, in *Problems of Physics and Evolution of the Universe*, ed. L. V. Mirzoyan (Yerevan: Publ. Armenian Academy of Sciences), 171
- Herczeg, G. J., Cruz, K. L., & Hillenbrand, L. A. 2009, *ApJ*, 696, 1589
- Herczeg, G. J., & Hillenbrand, L. A. 2014, *ApJ*, 786, 97
- Herczeg, G. J., & Hillenbrand, L. A. 2015, *ApJ*, 808, 23
- Hernández, J., Hartmann, L., Megeath, T., et al. 2007, *ApJ*, 662, 1067
- Hook, I., Jørgensen, I., Allington-Smith, J. R., et al. 2004, *PASP*, 116, 425
- Houk, N. 1982, *Michigan Catalogue of Two-dimensional Spectral Types for the HD Stars. Vol. 3*, (Ann Arbor: Univ. Mich.)
- Houk, N., & Smith-Moore, M. 1988, *Michigan Catalogue of Two-dimensional Spectral Types for the HD Stars. Vol. 4*, (Ann Arbor: Univ. Mich.)
- Jensen, E. L. N., Cohen, D. H., & Neuhäuser, R. 1998, *AJ*, 116, 414
- Johnson, D. R. H., & Soderblom, D. R., 1987, *AJ*, 93, 864
- Jura, M. 1991, *ApJ*, 383, L79
- Kastner, J. H., Zuckerman, B., & Bessell, M. 2008, *A&A*, 491, 829
- Kastner, J. H., Zuckerman, B., Weintraub, D. A., & Forveille, T. 1997, *Science*, 277, 67
- Kaufer, A., Stahl, O., Tubbesing, S., et al. 1999, *The Messenger*, 95, 8
- Kellogg, K., Metchev, S., Gagné, J., & Faherty, J. 2016, *ApJ*, 821, L15
- Kellogg, K., Metchev, S., Geißler, K., et al. 2015, *AJ*, 150, 182
- Kenyon, S. J., & Bromley, B. C. 2005, *AJ*, 130, 269
- Kidder, B., Mace, G., Sokal, K., Lopez, R., & Jaffe, D. 2019, *ApJ*, 879, 63
- Kirkpatrick, J. D., Henry, T. J., & Irwin, M. J. 1997, *AJ*, 113, 1421
- Kirkpatrick, J. D., Henry, T. J., & McCarthy, D. W. 1991, *ApJS*, 77, 417
- Kraus, A. L., Cody, A. M., Covey, K. R., et al. 2015, *ApJ*, 807, 3
- Lada, C. J. 1987, in *IAU Symp. 115, Star Forming Regions*, ed. M. Peimbert & J. Jugaku (Dordrecht: Reidel), 1
- Lada, C. J., & Wilking, B. A. 1984, *ApJ*, 287, 610
- Lindgren, L. 2018, *Re-normalising the astrometric chi-square in Gaia DR2*, GAIA-C3-TN-LU-LL-124-01, http://www.rssd.esa.int/doc_fetch.php?id=3757412
- Looper, D. L. 2011, PhD thesis, Univ. Hawai'i

- Looper, D. L., Bochanski, J. J., Burgasser, A. J., et al. 2010b, *AJ*, 140, 1486
- Looper, D. L., Burgasser, A. J., Kirkpatrick, J. D., & Swift, B. J. 2007, *ApJ*, 669, L97
- Looper, D. L., Mohanty, S., Bochanski, J. J., et al. 2010a, *ApJ*, 714, 45
- Low, F. J., Smith, P. S., Werner, M., et al. 2005, *ApJ*, 631, 1170
- Luhman, K. L. 1999, *ApJ*, 525, 466
- Luhman, K. L. 2022a, *AJ*, 163, 24
- Luhman, K. L. 2022b, *AJ*, 163, 25
- Luhman, K. L. 2022c, *AJ*, 164, 151
- Luhman, K. L. 2023, *AJ*, 165, 37
- Luhman, K. L., Allen, P. R., Espaillat, C., Hartmann, L., & Calvet, N. 2010, *ApJS*, 186, 111
- Luhman, K. L., & Esplin, T. L. 2020, *AJ*, 160, 44
- Luhman, K. L., Liebert, J., & Rieke, G. H. 1997, *ApJ*, 489, L165
- Luhman, K. L., & Mamajek, E. E. 2012, *ApJ*, 758, 31
- Luhman, K. L., Mamajek, E. E., Shukla, S. J., & Loutrel, N. P. 2017, *AJ*, 153, 46
- MacDonald, J., & Mullan, D. J. 2017, *ApJ*, 834, 67
- Makarov, V. V., Gaume, R. A., & Andrievsky, S. M. 2005, *MNRAS*, 362, 1109
- Malo, L., Artigau, É, Doyon, R., et al. 2014, *ApJ*, 788, 81
- Mamajek, E. E. 2005, *ApJ*, 634, 1385
- Mamajek, E. E., & Bell, C. P. M. 2014, *MNRAS*, 445, 2169
- Manara, C. F., Testi, L., Rigliaco, E., et al. 2013, *A&A*, 551, A107
- Manjavacas, E., Bonnefoy, M., Schlieder, J. E., et al. 2014, *A&A*, 564, A55
- Mentuch, E., Brandeker, A., van Kerkwijk, M. H., Jayawardhana, R., & Hauschildt, P. H. 2008, *ApJ*, 689, 1127
- Miret-Roig, N., Galli, P. A. B., Brandner, W., et al. 2020, *A&A*, 642, A179
- Mohanty, S., Jayawardhana, R., & Barrado y Navascués, D. 2003, *ApJ*, 593, L109
- Mohanty, S., Jayawardhana, R., Huéramo, N., & Mamajek, E. 2007, *ApJ*, 657, 1064
- Morrow, A. L., Luhman, K. L., Espaillat, C., et al. 2008, *ApJ*, 676, L143
- Murphy, S. J., Lawson, W. A., & Bento, J. 2015, *MNRAS*, 453, 2220
- Muzerolle, J., Calvet, N., Briceño, C., Hartmann, L., & Hillenbrand, L. 2000, *ApJ*, 535, L47
- Neuhäuser, R., Guenther, E. W., Petr, M. G., et al. 2000, *A&A*, 360, L39
- Patience, J., King, R. R., De Rosa, R. J., & Marois, C. 2010, *A&A*, 517, A76
- Pecaut, M. J., & Mamajek, E. E. 2013, *ApJS*, 208, 9
- Perryman, M. A. C., de Boer, K. S., Gilmore, G., et al. 2001, *A&A*, 369, 339
- Price-Whelan, A. 2021, *adrn/pyia: v1.3*, Zenodo, doi:10.5281/zenodo.5057363
- Rebull, L. M., Stapelfeldt, K. R., Werner, M. W., et al. 2008, *ApJ*, 681, 1484
- Reid, N. 2003, *MNRAS*, 342, 837
- Reid, I. N., Cruz, K. L., Kirkpatrick, J. D., et al. 2008, *AJ*, 136, 1290
- Riaz, B., & Gizis, J. E. 2008, *ApJ*, 681, 1584
- Riaz, B., Gizis, J. E., & Harvin, J. 2006a, *AJ*, 132, 866
- Riaz, B., Gizis, J. E., & Hmiel, A. 2006b, *ApJ*, 639, L79
- Riedel, A. R., Alam, M. K., Rice, E. L., Cruz, K. L., & Henry, T. J. 2017, *ApJ*, 840, 87
- Riedel, A. R., Finch, C. T., Henry, T. J., et al. 2014, *AJ*, 147, 85
- Rieke, G. H., Su, K. Y. L., Stansberry, J. A., et al. 2005, *ApJ*, 620, 1010
- Rieke, G. H., Young, E. T., Engelbracht, C. W., et al. 2004, *ApJS*, 154, 25
- Riello, M., De Angeli, F., Evans, D. W., et al. 2021, *A&A*, 649, A3
- Rodriguez, D. R., Bessell, M. S., Zuckerman, B., & Kastner, J. H. 2011, *ApJ*, 727, 62
- Rodriguez, D. R., van der Plas, G., Kastner, J. H., et al. 2015, *A&A*, 582, L5
- Rucinski, S. M., & Krautter, J. 1983, *A&A*, 121, 217
- Schneider, A. C., Melis, C., & Song, I. 2012a, *ApJ*, 754, 39
- Schneider, A. C., Song, I., Melis, C., Zuckerman, B., & Bessell, M. 2012b, *ApJ*, 757, 163
- Schneider, A. C., Shkolnik, E. L., Allers, K. N., et al. 2019, *AJ*, 157, 234
- Schneider, A. C., Windsor, J., Cushing, M. C., Kirkpatrick, J. D., & Wright, E. L. 2016, *ApJ*, 822, L1
- Scholz, R.-D., McCaughrean, M. J., Zinnecker, H., & Lodieu, N. 2005, *A&A*, 430, L49
- Shkolnik, E. L., Allers, K. N., Kraus, A. L., Liu, M. C., & Flagg, L. 2017, *AJ*, 154, 69
- Shkolnik, E., Liu, M. C., Reid, I. N., Dupuy, T., & Weinberger, A. J. 2011, *ApJ*, 727, 6
- Skrutskie, M., Cutri, R. M., Stiening, R., et al. 2003, 2MASS All-Sky Point Source Catalog, IPAC, doi:10.26131/IRSA2
- Skrutskie, M., Cutri, R. M., Stiening, R., et al. 2006, *AJ*, 131, 1163
- Soderblom, D. R., Henry, T. J., Shetrone, M. D., Jones, B. F., & Saar, S. H. 1996, *ApJ*, 460, 984
- Soderblom, D. R., King, J. R., Siess, L., et al. 1998, *ApJ*, 498, 385
- Song, I., Zuckerman, B., & Bessell, M. S. 2003, *ApJ*, 599, 342
- Stauffer, J., Hartmann, L. W., & Barrado y Navascués, D. 1995, *ApJ*, 454, 910
- Stauffer, J. R., Schultz, G., & Kirkpatrick, J. D. 1998, *ApJ*, 499, L199
- Sterzik, M. F., Alcalá, J. M., Covino, E., & Petr, M. G. 1999, *A&A*, 346, L41
- Sterzik, M. F., Pascucci, I., Apai, D., van der Blik, N., & Dullemond, C. P. 2004, *A&A*, 427, 245
- Teixeira, R., Ducourant, C., Chauvin, G., et al. 2008, *A&A*, 489, 825
- Torres, C. A. O., da Silva, L., Quast, G. R., de la Reza, R., & Jilinski, E. 2000, *AJ*, 120, 1410
- Torres, C. A. O., Quast, G. R., da Silva, L., et al. 2006, *A&A*, 460, 695
- Torres, G., Guenther, E. W., Marschall, L. A., et al. 2003, *AJ*, 125, 825
- Uchida, K. I., Calvet, N., Hartmann, L., et al. 2004, *ApJS*, 154, 439
- Vacca, W. D., & Sandell, G. 2011, *ApJ*, 732, 8
- Venuti, L., Stelzer, B., Alcalá, J. M., et al. 2019, *A&A*, 632, A46
- Webb, R. A., Zuckerman, B., Platais, I., et al. 1999, *ApJ*, 512, L63
- Weinberger, A. J., Anglada-Escudé, G., & Boss, A. P. 2013, *ApJ*, 762, 118
- Werner, M. W., Roellig, T. L., Low, F. J., et al. 2004, *ApJS*, 154, 1
- White, R. J., & Hillenbrand, L. A. 2004, *ApJ*, 616, 998
- Wright, E. L., Eisenhardt, P. R., Mainzer, A. K., et al. 2010, *AJ*, 140, 1868
- Wright, E. L., Eisenhardt, P. R. M., Mainzer, A. K., et al. 2013, AllWISE Source Catalog, IPAC, doi:10.26131/IRSA1
- Zari, E., Brown, A. G. A., & de Zeeuw, P. T. 2019, *A&A*, 628, A123
- Zuckerman, B., & Becklin, E. E. 1993, *ApJ*, 406, L25
- Zuckerman, B., & Song, I. 2004, *ARA&A*, 42, 685
- Zuckerman, B., Webb, R. A., Schwartz, M., & Becklin, E. E. 2001, *ApJ*, 549, L233
- Zúñiga-Fernández, S., Bayo, A., Elliott, P., et al. 2021a, *A&A*, 645, A30
- Zúñiga-Fernández, S., Olofsson, J., Bayo, A., et al. 2021b, *A&A*, 655, A15

TABLE 1
NEW SPECTRAL CLASSIFICATIONS FOR CANDIDATE MEMBERS OF TWA

Gaia DR3	Spectral Type	$W_\lambda(\text{Li})^a$ (Å)	Instrument	Date
5414158429569765632	M3.5	0.48	FEROS	2013 Feb 17
5397574190745629312	M4	0.55	FEROS	2013 Feb 17
6183591791897683584	M4	0.47	FEROS	2013 Feb 17
6133420114251217664	M5.5	0.45	UVES	2013 Dec 27
6145303429765430784	M4.9	0.80	GMOS	2014 Feb 22
3493814268751183744	M5.75	0.64	GMOS	2023 Mar 5
5348165127505382400	M4.75	0.60	GMOS	2023 Mar 5
5401389770971149568	M6	...	GMOS	2023 Mar 5
6114656192408518784	M4.6	0.58	GMOS	2023 Mar 5
6143632653128880896	M4.9	0.72	GMOS	2023 Mar 5
6143984423832713856	M4.25	<0.1	GMOS	2023 Mar 5
6143984428129994624	M4.6	<0.1	GMOS	2023 Mar 5
6179256348830614784	M4.75	0.65	GMOS	2023 Mar 5

^a Typical uncertainties are 0.05 Å.

TABLE 2
ADOPTED MEMBERS OF TWA

Column Label	Description
GaiaDR3 Name	Gaia DR3 source name Other source name
RAdeg	Gaia DR3 right ascension (ICRS at Epoch 2016.0)
DEdeg	Gaia DR3 declination (ICRS at Epoch 2016.0)
SpType	Spectral type
r_SpType	Spectral type reference ^a
Adopt	Adopted spectral type
pmRA	Gaia DR3 proper motion in right ascension
e_pmRA	Error in pmRA
pmDec	Gaia DR3 proper motion in declination
e_pmDec	Error in pmDec
plx	Gaia DR3 parallax
e_plx	Error in plx
rmedgeo	Median of geometric distance posterior (Bailer-Jones et al. 2021)
rlogeo	16th percentile of geometric distance posterior (Bailer-Jones et al. 2021)
rhigeo	84th percentile of geometric distance posterior (Bailer-Jones et al. 2021)
RVel	Radial velocity
e_RVel	Error in RVel
r_RVel	Radial velocity reference ^b
U	U component of space velocity
e_U	Error in U
V	V component of space velocity
e_V	Error in V
W	W component of space velocity
e_W	Error in W
Gmag	Gaia DR3 G magnitude
e_Gmag	Error in Gmag
GBPmag	Gaia DR3 G_{BP} magnitude
e_GBPmag	Error in GBPmag
GRPmag	Gaia DR3 G_{RP} magnitude
e_GRPmag	Error in GRPmag
RUWE	Gaia DR3 renormalized unit weight error
2m	Closest 2MASS source within $3''$
2mseps	Angular separation between Gaia DR3 (epoch 2000) and 2MASS
2mclosest	Is this Gaia source the closest match for the 2MASS source?
wise	Closest WISE source within $3''$
wisesepp	Angular separation between Gaia DR3 (epoch 2010.5) and WISE
wiseclosest	Is this Gaia source the closest match for the WISE source?
Jmag	2MASS J magnitude
e_Jmag	Error in Jmag
Hmag	2MASS H magnitude
e_Hmag	Error in Hmag
Ksmag	2MASS K_s magnitude
e_Ksmag	Error in Ksmag
W1mag	WISE W1 magnitude
e_W1mag	Error in W1mag
W2mag	WISE W2 magnitude
e_W2mag	Error in W2mag
f_W2mag	Flag on W2mag ^c
W3mag	WISE W3 magnitude
e_W3mag	Error in W3mag
f_W3mag	Flag on W3mag ^c
W4mag	WISE W4 magnitude
e_W4mag	Error in W4mag
f_W4mag	Flag on W4mag ^c
ExcW2	Excess present in W2?
ExcW3	Excess present in W3?
ExcW4	Excess present in W4? ^d
DiskType	Disk type
bfmem	Bona fide member of TWA from Gagné et al. (2017)
outlier	Spatial outlier

TABLE 2 — *Continued*

Column Label	Description
--------------	-------------

NOTE. — The table is available in its entirety in machine-readable form.

^a (1) Schneider et al. (2019); (2) Riedel et al. (2014); (3) Riedel et al. (2017); (4) this work; (5) Rodriguez et al. (2011); (6) Riaz et al. (2006a); (7) Schneider et al. (2012b); (8) Gagné et al. (2015); (9) Murphy et al. (2015); (10) Luhman et al. (2017); (11) Webb et al. (1999); (12) Torres et al. (2006); (13) Manara et al. (2013); (14) Pecaut & Mamajek (2013); (15) Herczeg & Hillenbrand (2014); (16) Gagné et al. (2017); (17) Herbig (1978); (18) de la Reza et al. (1989); (19) Torres et al. (2000); (20) Vacca et al. (2011); (21) Venuti et al. (2019); (22) Scholz et al. (2005); (23) Allers & Liu (2013); (24) Looper (2011); (25) Houk (1982); (26) Cannon & Pickering (1993); (27) Bidelman et al. (1988); (28) Abt & Morrell (1995); (29) Shkolnik et al. (2011); (30) Sterzik et al. (1999); (31) Houk & Smith-Moore (1988); (32) Hawley et al. (1996); (33) Soderblom et al. (1996); (34) Neuhäuser et al. (2000); (35) Bonnefoy et al. (2014); (36) Binks et al. (2020); (37) Looper et al. (2010b); (38) Looper et al. (2010a); (39) White & Hillenbrand (2004); (40) Gizis (2002); (41) Looper et al. (2007); (42) Reid et al. (2008); (43) Bowler et al. (2019); (44) Zuckerman & Song (2004); (45) Herczeg et al. (2009); (46) Gagné et al. (2014); (47) Reid (2003); (48) Zuckerman et al. (2001); (49) Kastner et al. (2008); (50) Stauffer et al. (1995); (51) Manjavacas et al. (2014).

^b (1) Schneider et al. (2019); (2) Gaia DR3; (3) Buder et al. (2018); (4) Gagné et al. (2017); (5) Bailey et al. (2012); (6) Murphy et al. (2015); (7) Fouqué et al. (2018); (8) Zúñiga-Fernández et al. (2021a); (9) Shkolnik et al. (2011); (10) Zúñiga-Fernández et al. (2021b); (11) Torres et al. (2003); (12) Mohanty et al. (2003); (13) Looper et al. (2010b); (14) Looper et al. (2010a); (15) Venuti et al. (2019); (16) Reid (2003); (17) Elliott et al. (2014); (18) Kidder et al. (2019).

^c nodet = nondetection; false = detection from AllWISE appears to be false or unreliable based on visual inspection.

^d Excess classifications in W4 for TWA 8B and TWA 26 are based on 24 μ m photometry from the Spitzer Space Telescope (Luhman et al. 2010).

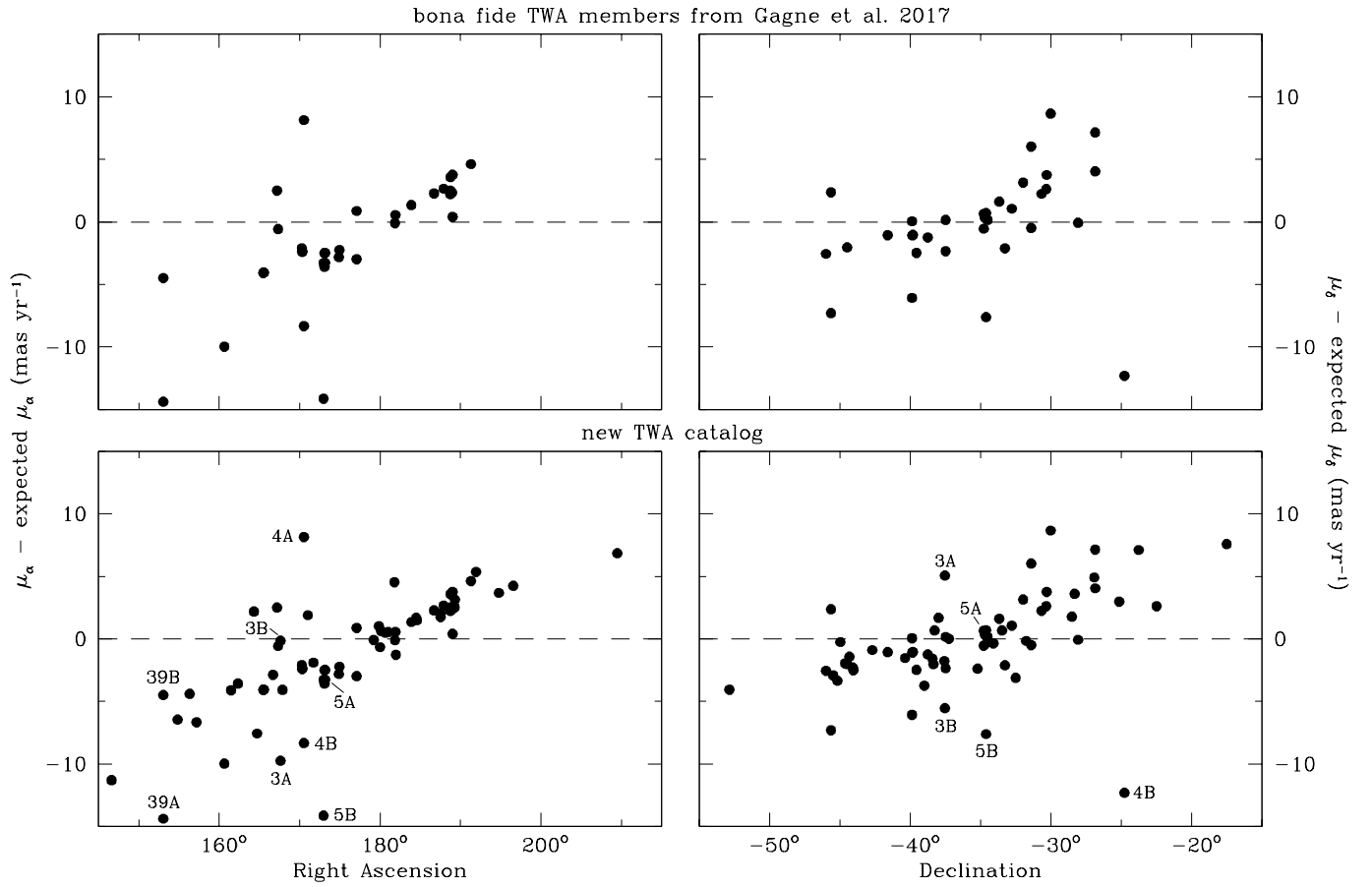


FIG. 1.— Proper motion offsets versus equatorial coordinates for the bona fide members of TWA compiled by Gagné et al. (2017) (top) and the adopted members from this work (bottom). Outliers are labeled with their TWA numbers. TWA 4A is beyond the boundaries of the diagrams on the right.

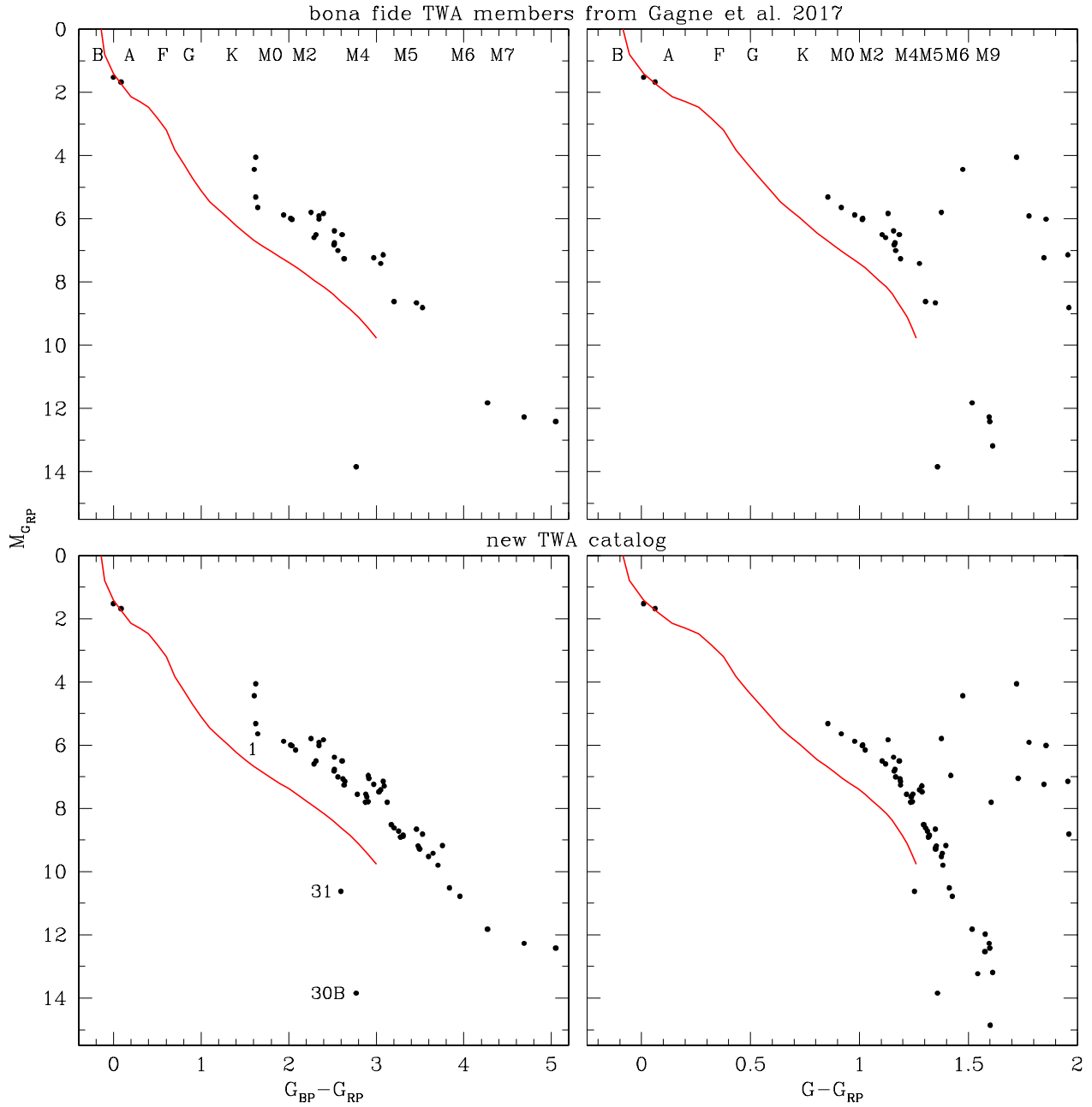


FIG. 2.— $M_{G_{RP}}$ versus $G_{BP} - G_{RP}$ and $G - G_{RP}$ for the bona fide members of TWA compiled by Gagné et al. (2017) (top) and the adopted members from this work (bottom). Three stars that appear below the sequence in $G_{BP} - G_{RP}$ are labeled with their TWA numbers. Each CMD includes a fit to the single-star sequence of the Pleiades (red line, Luhman 2023). The spectral types that correspond to the colors of young stars are indicated in the top CMDs (Luhman 2022a).

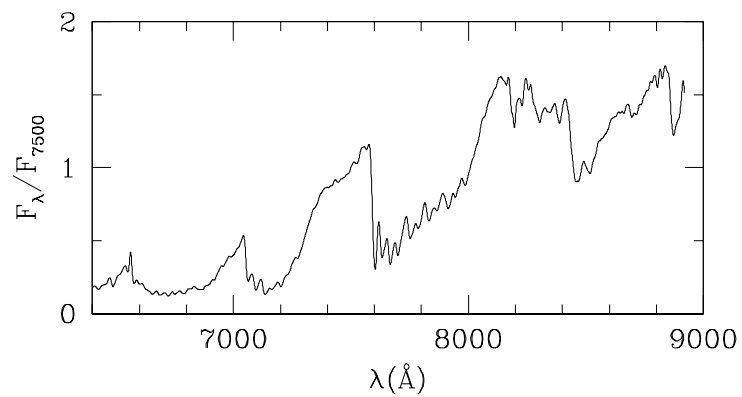


FIG. 3.— Example of a GMOS spectrum of a candidate member of TWA (Gaia DR3 5401389770971149568), which is displayed at a resolution of 13 \AA . The data used to create this figure are available.

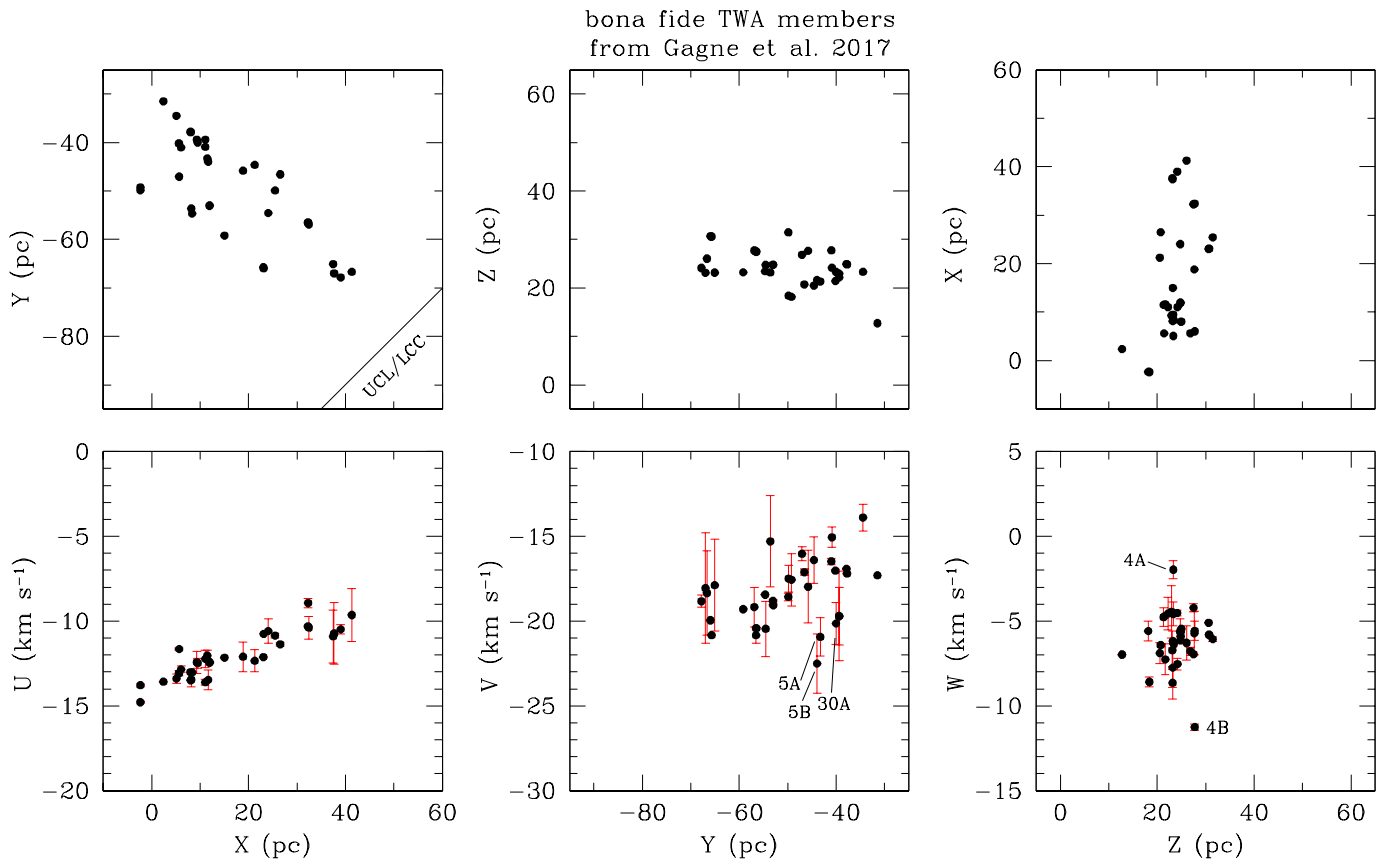


FIG. 4.— Galactic Cartesian coordinates and UVW velocities for the bona fide members of TWA compiled by Gagné et al. (2017). The most discrepant measurements of UVW are labeled with the TWA numbers.

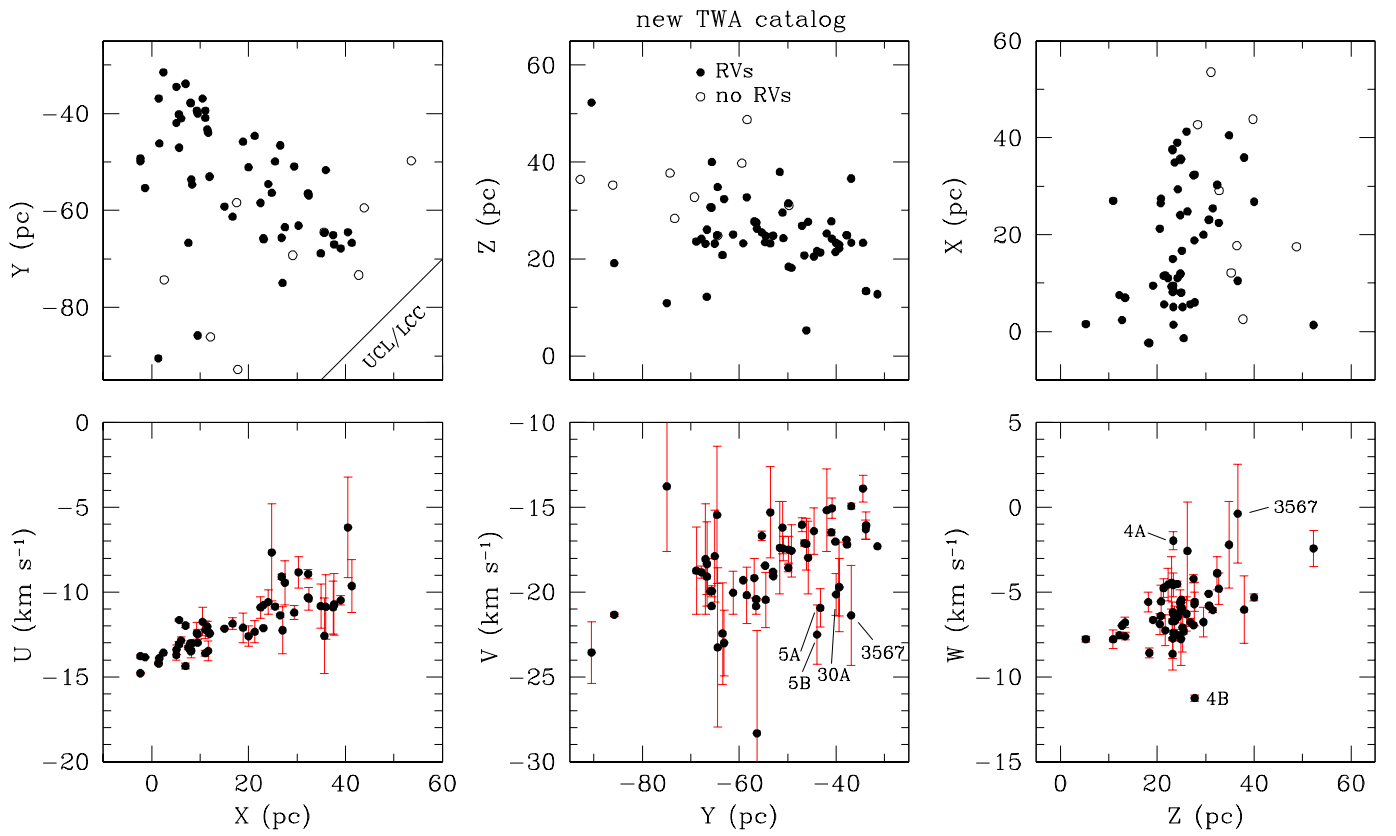


FIG. 5.— Galactic Cartesian coordinates and UVW velocities for adopted members of TWA from this work. The most discrepant measurements of UVW are labeled with the TWA numbers. The V and W velocities of Gaia DR3 3567379121431731328 are also marked. Its membership is discussed in Section 2.3.

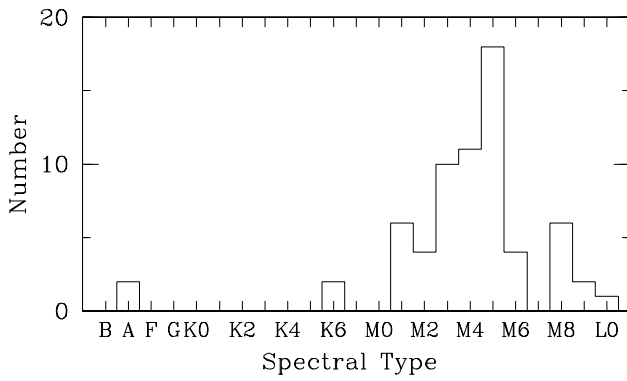


FIG. 6.— Histogram of spectral types for adopted members of TWA.

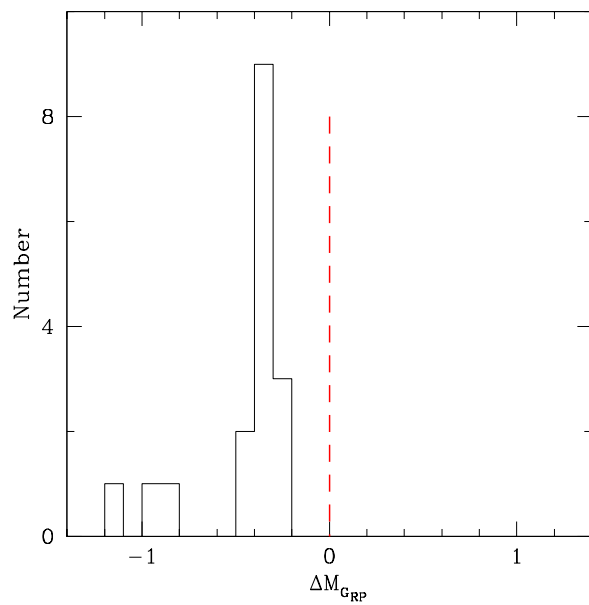


FIG. 7.— Histogram of offsets in M_{GRP} from the median CMD sequence for UCL/LCC for low-mass stars in TWA (Figure 2). Negative values correspond to brighter magnitudes and younger ages.

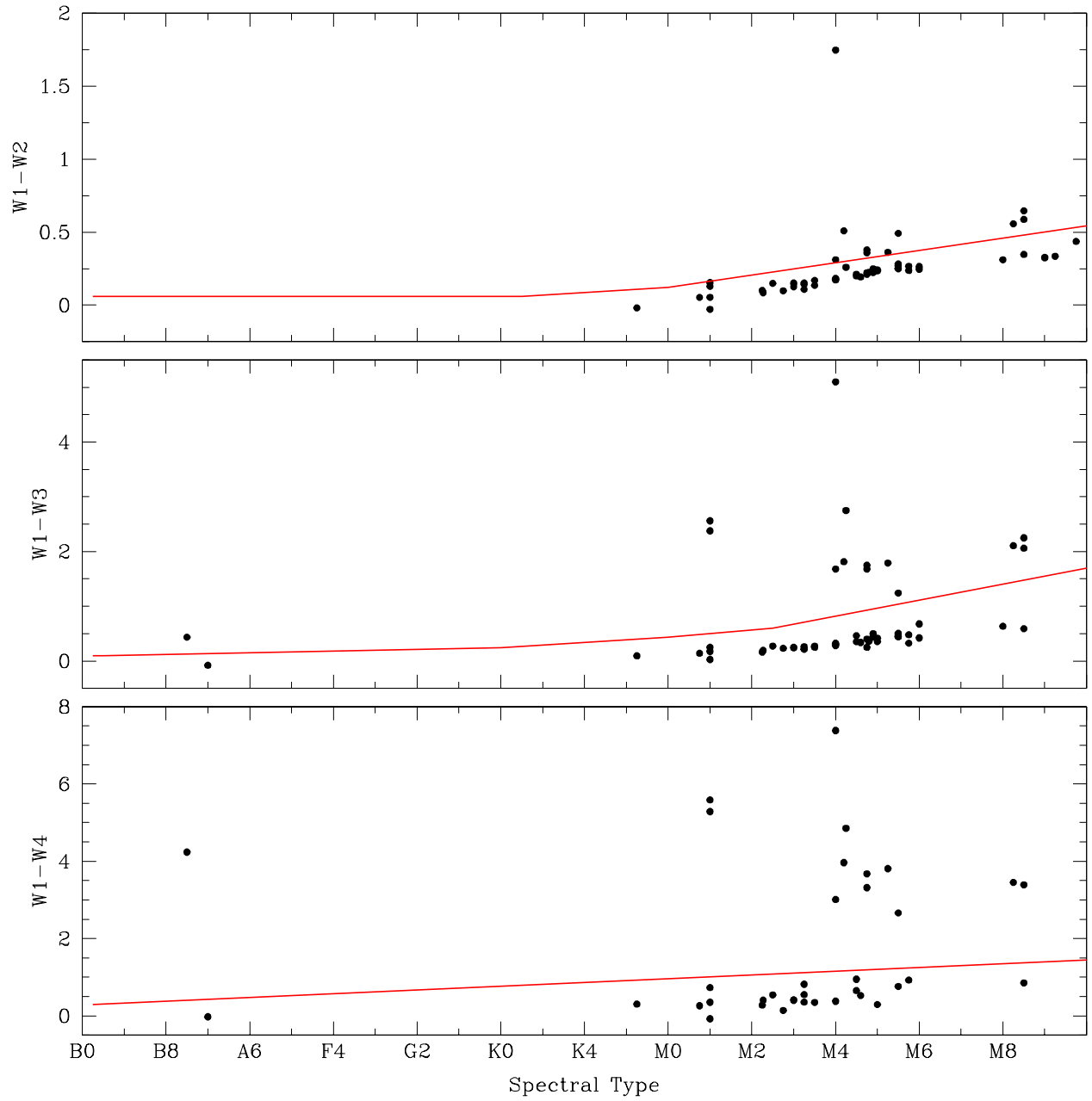


FIG. 8.— IR colors versus spectral type for adopted members of TWA. In each diagram, the tight sequence of blue colors corresponds to stellar photospheres. The thresholds used for identifying color excesses from disks are indicated (red solid lines, Luhman 2022b).

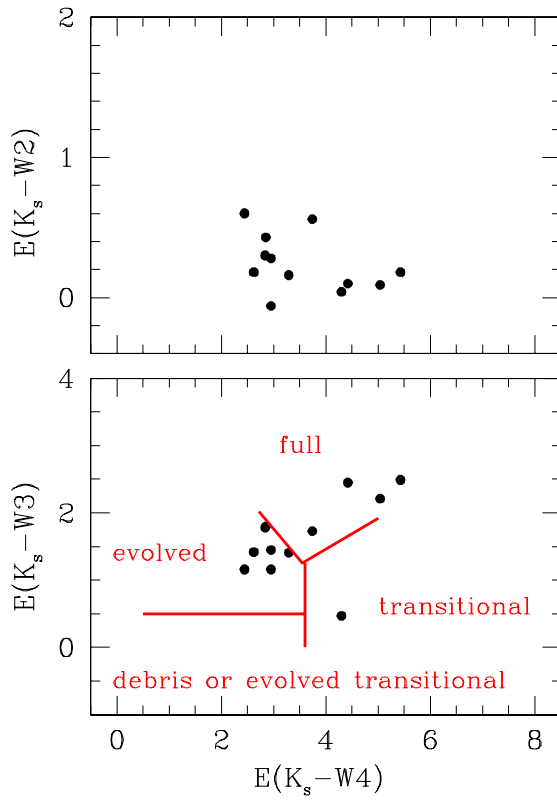


FIG. 9.— IR color excesses for adopted members of TWA. The boundaries used for assigning disk classes are shown in the bottom diagram (red solid lines).